

Chapter 3: Probing the Dynamics of *O*-GlcNAc Glycosylation in the Brain Using Quantitative Proteomics

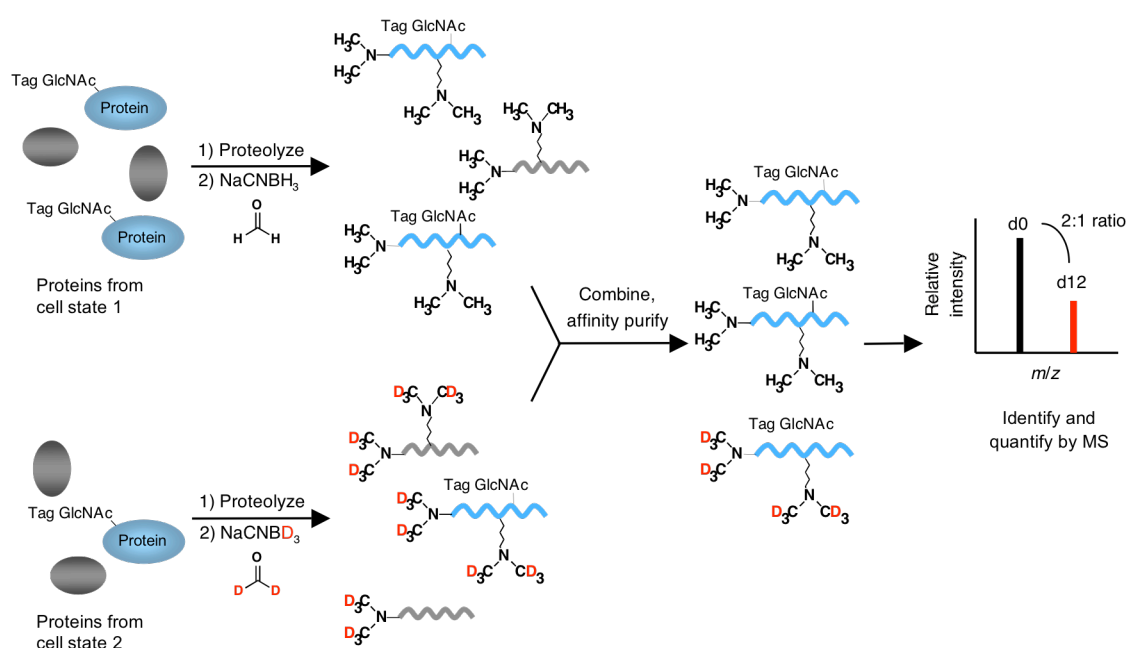
Portions of this chapter are from Khidekel, N., Ficarro, S.B., Clark, P.M., Bryan, M.C., Swaney, D.L., Rexach, J.E., Sun, Y.E., Coon, J.J., Peters, E.C. & Hsieh-Wilson, L.C. Probing the dynamics of *O*-GlcNAc glycosylation in the brain using quantitative proteomics. *Nat. Chem. Biol.* **3**, 339-48 (2007).

The addition of the monosaccharide β -*N*-acetyl-D-glucosamine to proteins (*O*-GlcNAc glycosylation) is an intracellular, post-translational modification that shares features with phosphorylation. Here, we demonstrate a new strategy for monitoring the dynamics of *O*-GlcNAc glycosylation using quantitative mass spectrometry-based proteomics. Our method, termed QUIC-tag, combines selective, chemoenzymatic tagging of *O*-GlcNAc proteins with an efficient isotopic labeling strategy. A key advantage of the approach is that it can be applied to post-mitotic cells such as neurons after *in vivo* stimulation. Using the method, we detect changes in *O*-GlcNAc glycosylation on several proteins involved in the regulation of transcription and mRNA translocation. We also provide the first evidence that *O*-GlcNAc glycosylation is dynamically modulated by excitatory stimulation of the brain *in vivo*. Finally, we employ electron transfer dissociation (ETD) mass spectrometry to identify exact sites of *O*-GlcNAc modification. Together, our studies suggest that *O*-GlcNAc glycosylation occurs reversibly in neurons and, akin to phosphorylation, may play important roles in mediating the communication between neurons.

The QUIC-Tag Strategy for *O*-GlcNAc Peptide Identification and Quantification

As the majority of peptides from a biological sample are not post-translationally modified, detection of a specific modification by MS requires an enrichment strategy to isolate peptides containing the modification of interest from other species. We reasoned that our chemoenzymatic strategy (**Chapter 1, Fig. 2a**)¹ could be combined with differential isotopic labeling to allow for the first direct, high-throughput quantification of

O-GlcNAc dynamics on specific proteins. In this approach, which we have termed Quantitative Isotopic and Chemoenzymatic Tagging (QUIC-Tag), lysates from two cellular states (e.g., stimulated vs. unstimulated, diseased vs. normal) were chemoenzymatically labeled and proteolytically digested (**Scheme 1**). A modified dimethyl labeling strategy² incorporated stable isotopes into peptide N-terminal amines and ϵ -amino groups of lysine residues by reductive amination for subsequent MS quantification. Treatment with either formaldehyde/NaCNBH₃ or deuterated formaldehyde/NaCNBD₃ created mass differences of $6 \times n$ between the peptides from the two cell populations, where n is the number of primary amine functionalities in the peptide. This allowed for complete resolution of isotopic envelopes even at higher charge states (i.e., +4) during MS analysis. Following isotopic labeling, we combined



Scheme 1: QUIC-Tag strategy for quantitative *O*-GlcNAc proteomics. *O*-GlcNAc proteins from two different cell states are selectively tagged, proteolyzed and differentially labeled with ‘light’ or ‘heavy’ isotopes. The mixtures are combined, and *O*-GlcNAc peptides of interest are specifically enriched by avidin chromatography for selective quantification by LC-MS.

and enriched the peptides from both populations by affinity chromatography for the presence of *O*-GlcNAc. Relative quantification of *O*-GlcNAc glycosylation in the two cellular states was accomplished by calculation of the chromatographic peak area as determined by the MS response to each eluting glycosylated pair of peptide ions.

Quantification of Known *O*-GlcNAc Peptides from Complex Mixtures

Nelly Khidekel first evaluated the effectiveness of the dimethyl labeling strategy using the model protein α -casein. α -casein was digested with trypsin, and the resulting peptides were reacted with formaldehyde and NaCNBH₃ at pH values ranging from 5-8. Liquid chromatography-mass spectrometry (LC-MS) analysis of the labeled peptides indicated that reductive amination proceeded quantitatively for both lysine and N-terminal primary amines in less than 10 min at pH 7 (data not shown). In contrast to previous studies², we observed that higher pH values were necessary to achieve complete labeling of basic lysine residues.

Having established the optimal conditions for dimethyl labeling, Nelly investigated our ability to capture and quantify known *O*-GlcNAc peptides^{3, 4} from complex mixtures. Known amounts of the proteins α -crystallin (ca. 300 pmol) and OGT (ca. 10 pmol) were added to two samples of rat brain lysate. We chose to examine α -crystallin because of its low stoichiometry of glycosylation (<10%) and because it has represented a formidable challenge for detection by several methods^{1, 5}. The samples were chemoenzymatically labeled, proteolytically digested, isotopically labeled and combined as described in **Scheme 1**. Following avidin capture of the *O*-GlcNAc peptides, Scott Ficarro performed relative quantification of glycosylated peptide pairs

using an orbitrap mass spectrometer⁶, which provided accurate mass (<20 ppm) and high resolution (100,000 at m/z 400) ion measurements. Precursor peptide cations that exhibited the signature loss of the labile ketogalactose-biotin and GlcNAc-ketogalactose-biotin groups during MS/MS were subjected to further fragmentation via MS⁴.

In these experiments, Nelly and Scott reproducibly captured and quantified 3 α -crystallin peptides that encompass all of the known glycosylation sites on both the A and B forms of α -crystallin^{3,7}. Additionally, Nelly captured 8 OGT peptides representing all

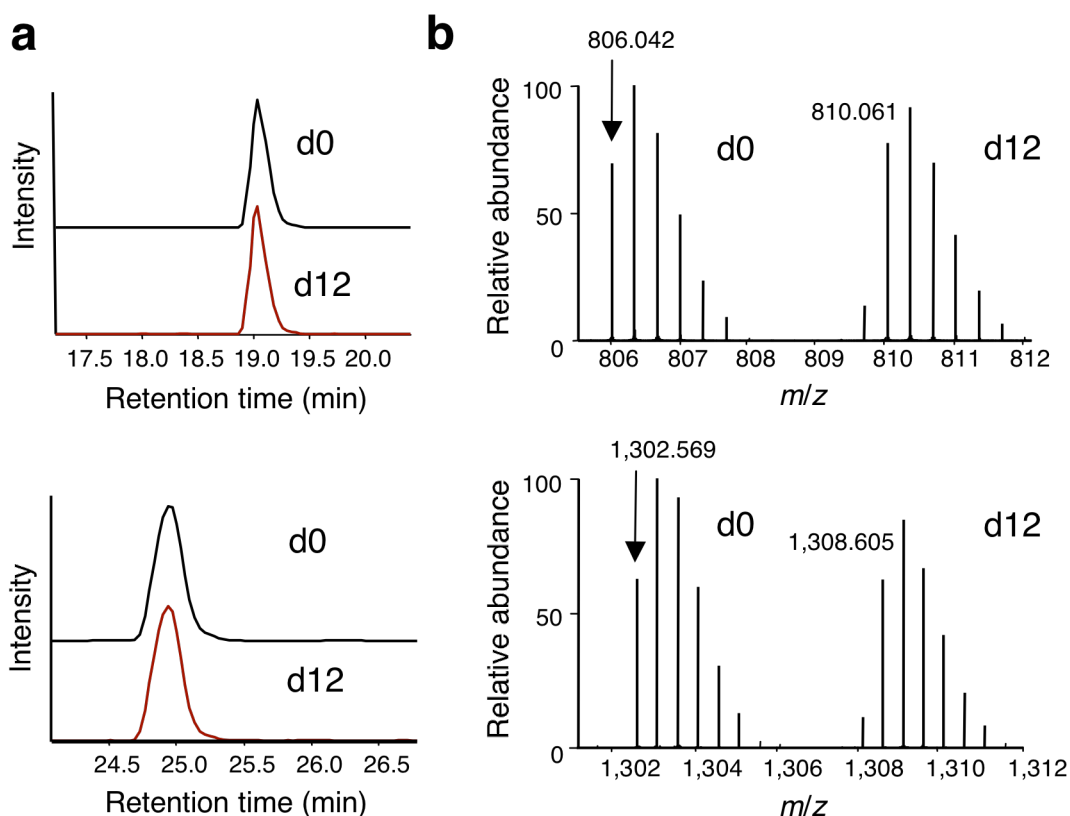


Figure 1: Accurate quantification of known *O*-GlcNAc peptides from complex mixtures using the QUIC-Tag approach. **(a)** Extracted ion chromatogram of the heavy and light forms of two representative *O*-GlcNAc glycosylated peptides, α -crystallin peptide ¹⁵⁸AIPVSREEKPSSAPSS¹⁷³ (top) and OGT peptide ³⁹⁰ISPTFADAYSNMGNTLK⁴⁰⁶ (bottom). Co-elution by reversed-phase liquid chromatography was observed. **(b)** Quantification from the isotopic cluster of the heavy (m/z 810.061) and light (m/z 806.416) forms of the α -crystallin peptide yields a heavy:light ratio of 0.97 – 0.09, 0.97 + 0.10 (g.s.d. of 1.10). Quantification of the heavy (m/z 1308.605) and light (m/z 1302.569) forms of the OGT peptide yields a heavy:light ratio of 0.93 – 0.12, 0.93 + 0.14 (g.s.d. of 1.15). Prior to labeling, both proteins were added to neuronal lysates at a ratio of 1:1. $n = 7$.

Table 1a Mean ratios of individual peptides from α -crystallin and OGT

Protein	Peptide Sequence	n	Ratio ^a	s.d. ^b
crystallin 1	AIPVSREEKPSSAPSS	7	0.97	± 0.10
crystallin 2	AIPVSREEKPSSAPS	7	0.90	± 0.13
crystallin 3	EEKPVVTAAPK	4	0.81	± 0.11
OGT 1	IKPVEVTESA	7	0.91	± 0.33
OGT 2	AIQINPAFADAHSNLAHSLASIHK	7	0.77	± 0.15
OGT 3	ISPTFADAYSNMGNLTK	7	0.93	± 0.14
OGT 4	EMQDVQGALQCYTR	5	0.98	± 0.11
OGT 5	AIQINPAFADAHSNLAHSLASIHKDSGNIPEAIASYSR	4	1.01	± 0.29
OGT 6	AIQINPAFADAHSNLAHSLASIHKDSGNIPEAIAS	3	0.72	± 0.15
OGT 7	AATGEEVPRTIIVTTR	7	0.96	± 0.18
OGT 8	EAIRISPTFADAYSNMGNLTK	2	1.12	± 0.18

^a Geometric mean^b Maximum absolute standard deviation (s.d.) calculated from g.s.d.**Table 1b Mean ratios of all peptides**

Experiment	Ratio ^a	s.d. ^b
1	0.83	± 0.07
2	0.90	± 0.28
3	0.80	± 0.15
4	1.01	± 0.27
5	0.94	± 0.17
6	0.96	± 0.20
7	0.89	± 0.17

^a Geometric mean^b Maximum absolute standard deviation (s.d.) calculated from g.s.d.

of the known glycosylation sites on OGT⁴. The results for two such peptides, ¹⁵⁸AIPVSREEKPSSAPSS¹⁷³ from α -crystallin and ³⁹⁰ISPTFADAYSNMGNLTK⁴⁰⁶ from OGT, are highlighted in **Figure 1**. The deuterated and non-deuterated peptides generally co-eluted during reversed-phase chromatography (**Fig. 1a**), minimizing the isotope resolution effects during LC previously reported to interfere with deuterium-labeled peptides^{2,8}. To quantify the relative amounts of each peptide, Nelly compared the ratio of signal intensities from the heavy to the light forms, across the entire chromatographic profile of each peptide (**Fig. 1b**). She observed the α -crystallin peptide at a mean heavy:light ratio of 0.97 – 0.09, 0.97 + 0.10 (geometric standard deviation (g.s.d) of 1.10) and the OGT peptide at a mean heavy:light ratio of 0.93 – 0.12, 0.93 + 0.14 (g.s.d. of 1.15). The geometric mean ratio and standard deviation obtained for each of the α -crystallin and OGT peptides is found in **Table 1a**, and the mean ratio of all quantified peptides for each of seven independent experiments is shown in **Table 1b**. The mean ratio across all peptides over the seven experiments was 0.91 – 0.17, 0.91 + 0.21 (g.s.d. of 1.23), which compares favorably with the quantitative accuracy of other approaches such as iTRAQ and SILAC (mean observed ratios of 1.03 ± 0.16 and 1.03 ± 0.17 for an expected 1:1 ratio, respectively)^{9, 10}.

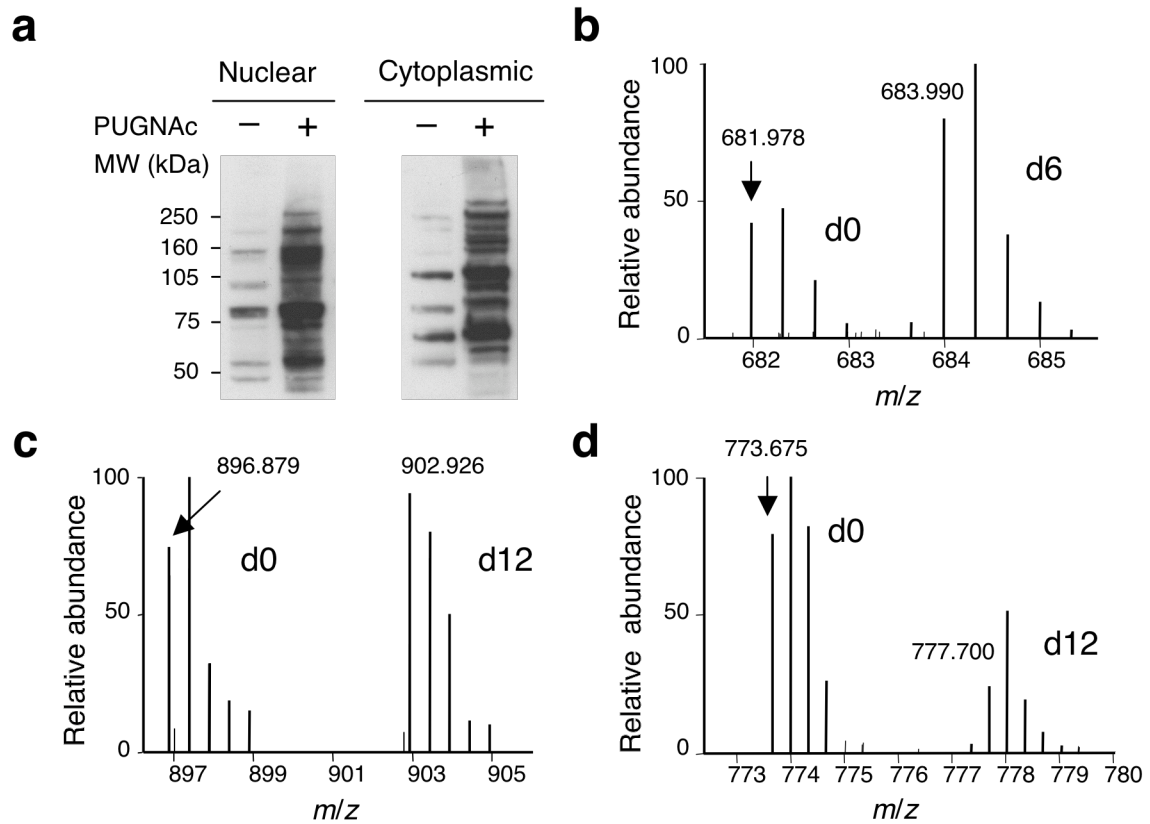


Figure 2: *O*-GlcNAc glycosylation is reversible in cultured cortical neurons. (a) Treatment of cortical neurons with the OGA inhibitor PUGNAc for 12 h enhances overall *O*-GlcNAc glycosylation levels in both nuclear and cytoplasmic fractions, as measured by immunoblotting with an anti-*O*-GlcNAc antibody. (b-d) Peptide mass spectra of three proteins displaying distinct activation profiles. *O*-GlcNAc glycosylation of the peptide in b was up-regulated in response to PUGNAc treatment, whereas the glycosylation level was unchanged for the peptide in c and was down-regulated for the peptide in d.

Probing the Reversibility of *O*-GlcNAc Glycosylation in Neurons using QUIC-Tag

We next applied the approach to study the reversibility of the *O*-GlcNAc modification in neurons. Although studies have suggested that *O*-GlcNAc levels can be modulated in various cell types^{11, 12}, the neuronal proteins that undergo reversible glycosylation are largely unknown. Nelly treated cultured cortical neurons from embryonic day-18 rats with the OGA inhibitor PUGNAc (*O*-(2-acetamido-2-deoxy-D-glucopyranosylidene)amino-*N*-phenylcarbamate)¹³ for 12 h. PUGNAc has been shown to

up-regulate global *O*-GlcNAc levels in neutrophils¹¹, kidney¹², and other cells by preventing the de-glycosylation of *O*-GlcNAc proteins. Consistent with these studies, Nelly found that PUGNAc strongly enhanced the overall levels of *O*-GlcNAc glycosylation in both the nuclear and S100 cytoplasmic fractions of cortical neurons, as demonstrated by Western blotting with an anti-*O*-GlcNAc antibody (**Fig. 2a**). To identify the proteins undergoing changes, neurons stimulated with and without PUGNAc were lysed and treated as outlined in **Scheme 1**. Prior to chemoenzymatic labeling, Nelly added known quantities of the standards α -crystallin and OGT into each lysate. Subsequent MS quantification focused on precursor ions that demonstrated characteristic

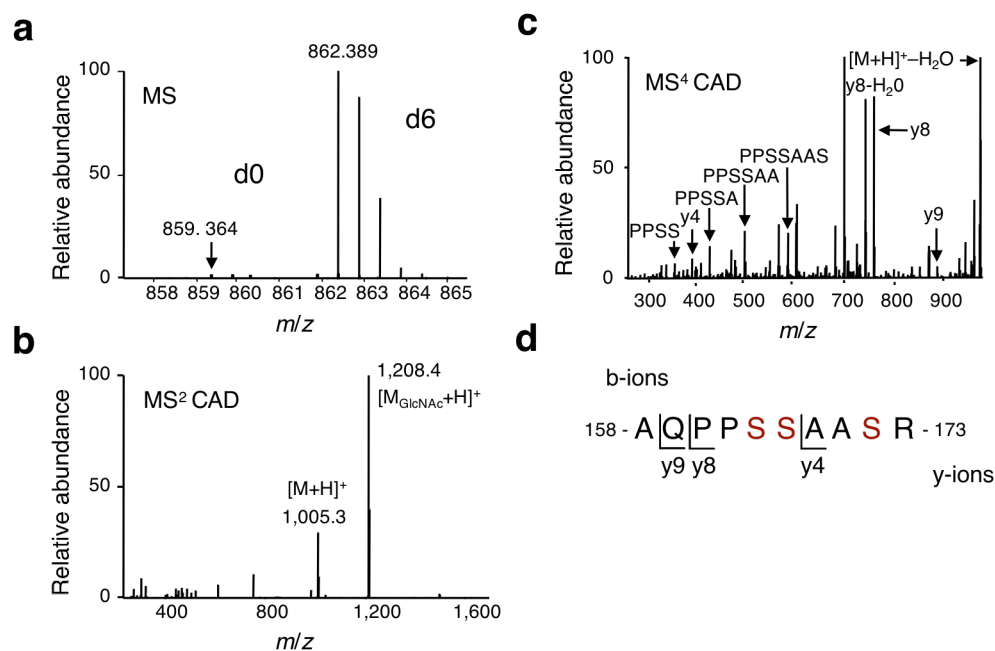


Figure 3: Sequencing of tagged *O*-GlcNAc peptides regulated by PUGNAc treatment using CAD. (a) MS spectrum of a representative peptide whose glycosylation level is significantly increased by PUGNAc treatment of cortical neurons. (b) MS/MS spectrum of the deuterated peak ($m/z = 862.389$), showing loss of a ketogalactose-biotin moiety ($m/z = 1208.4$) and GlcNAc-ketogalactose-biotin moiety ($m/z = 1005.3$). (c-d) Fragmentation during MS⁴ analysis yielded numerous internal cleavages and several prominent b and y ions that identified the peptide as ¹⁵⁸AQPPSSASSR¹⁷³ from eIF4G. The MS/MS spectrum of a derivatized synthetic peptide matched the MS⁴.

ketogalactose-biotin and GlcNAc-ketogalactose-biotin signature fragmentation patterns. To obtain the relative change in glycosylation on specific peptides, we corrected the heavy:light ratios using a normalization factor derived from the linear regression of the α -crystallin and OGT standard ratios within each sample. Analysis of standard peptides suggests that we could detect 1.15-fold changes in the nuclear sample and 1.70-fold changes in the cytoplasmic sample with 95% confidence (see Methods for statistical analysis). The peptide standards formed a normal distribution around the mean standard ratio as measured by the D'Agostino-Pearson omnibus test, suggesting that ratios greater than 2 standard deviations (σ) of the mean ratio are likely significant.

Using these criteria, 22 peptides from the nuclear sample and 11 peptides from the corresponding cytoplasmic sample showed an increase in *O*-GlcNAc glycosylation upon PUGNAc stimulation (**Fig. 2b**). Interestingly, we found that the presence of PUGNAc did not result in increased *O*-GlcNAc glycosylation on all proteins. For example, in the same nuclear sample, 4 *O*-GlcNAc peptides showed no measurable change in glycosylation, whereas in the cytoplasmic sample 16 peptides showed no measurable change (**Fig. 2c**). We also observed decreases in glycosylation on 5 nuclear and 4 cytoplasmic *O*-GlcNAc peptides (**Fig. 2d**). These site-dependent differences suggest differential regulation of the modification in cells, with some proteins being more susceptible to reversible cycling than others.

Identification of Proteins Subject to Reversible Glycosylation in Neurons

To identify the neuronal proteins undergoing reversible glycosylation, Scott targeted a portion of the *O*-GlcNAc peptides for sequencing by MS⁴ analysis. A

representative ESI-MS spectrum of an *O*-GlcNAc peptide whose glycosylation state was elevated upon PUGNAc treatment is shown (**Fig. 3a**). The CAD MS² spectrum of the deuterated, triply charged peptide ($m/z = 862.389$) displays a characteristic loss of a ketogalactose-biotin moiety ($m/z = 1208.4$) and GlcNAc-ketogalactose-biotin moiety ($m/z = 1005.3$) (**Fig. 3b**). MS⁴ analysis generated a series of b- and y-type product ions and internal cleavages that enabled definitive sequencing of the peptide (**Fig. 3c,d**). Database searching identified the peptide as belonging to the protein translation elongation initiation factor 4G (eIF4G).

To sequence *O*-GlcNAc-containing peptides and locate the exact sites of glycosylation, Nelly and Danielle Swaney also employed a recently reported fragmentation method, electron transfer dissociation (ETD)^{14, 15}. ETD utilizes small molecule radical anions to deliver electrons to isolated peptide precursor cations. After receiving the electron, the odd-electron peptide cation undergoes backbone fragmentation with minimal cleavage of amino acid side chains. This results in the production of sequence-specific c- and z-type product ions without the loss of labile post-translational modification — dissociation pathways that can dominate CAD spectra. As ETD has been successfully used to elucidate exact sites of phosphorylation¹⁴ and *N*-glycosylation¹⁶, we envisioned that it might be a powerful approach for mapping *O*-GlcNAc glycosylation sites. A representative ETD tandem mass spectrum of an *O*-GlcNAc-modified peptide whose glycosylation level was increased in the PUGNAc-treated sample is shown (**Fig. 4a**). ETD provided near complete sequence coverage for this peptide (**Fig. 4b**), belonging to the transcriptional repressor p66 β . Importantly, the *O*-GlcNAc linkage was preserved during ETD fragmentation, and we observed the added mass corresponding to the tagged

O-GlcNAc moiety on the c-type product ion series. The tagged *O*-GlcNAc-modified c3 ion narrowed the *O*-GlcNAc glycosylation site to the N-terminal Ser-584 or Ser-586 of this peptide (**Fig. 4c**). ETD was highly effective for the fragmentation of lower *m/z* GlcNAc-ketogalactose-biotin peptide precursor cations (e.g., < ~800), but was less effective for precursors above this *m/z* value. Recent work suggests supplemental collisional activation of the electron transfer product species can help counter this problem¹⁷.

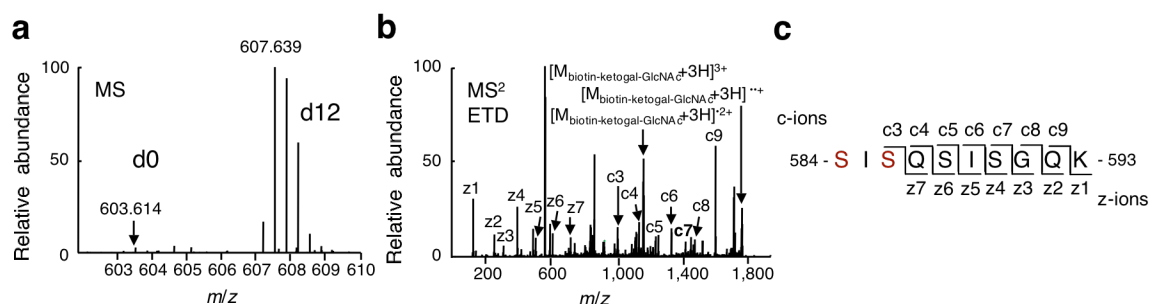


Figure 4: Sequencing of tagged *O*-GlcNAc peptides regulated by PUGNAc treatment using ETD. (a) MS spectrum of a second representative peptide whose glycosylation level is significantly enhanced in response to PUGNAc treatment of cortical neurons. (b, c) MS/MS analysis of the deuterated peak (*m/z* = 607.639) yielded c and z ions that identified the peptide as ⁵⁸⁴SISQISIGQK⁵⁹³ from the transcriptional repressor p66β. The presence of the tagged GlcNAc moiety on the c series of ions narrowed the site of glycosylation to Ser-584 or Ser-586.

Using a combination of CAD and ETD, Scott and Danielle sequenced 7 of the *O*-GlcNAc peptides that undergo significant increases in glycosylation upon PUGNAc treatment (**Table 2**). In addition, Danielle identified another peptide by ETD that was not observed in the orbitrap MS analysis and thus could not be quantified. Among the *O*-GlcNAc proteins subject to reversible glycosylation are the transcriptional coactivator SRC-1 and the zinc finger RNA-binding protein, which we had previously identified as *O*-GlcNAc glycosylated³. Here, we extend those findings by identifying the exact site of glycosylation on both proteins using ETD and by showing that glycosylation at those

sites occurs reversibly in neurons. We also identified an *O*-GlcNAc peptide on the RNA-binding protein nucleoporin 153, which had been previously shown to be *O*-GlcNAc glycosylated¹⁸, but whose glycosylated peptides were unknown. In addition to these, we identified reversible sites of modification on several new proteins, including the transcriptional repressor p66 β , translation factor eIF4G, and the neuron-specific transcriptional repressor BHC80. Finally, we found that the enzyme OGA is *O*-GlcNAc glycosylated in neurons, which is consistent with the ability of OGT to glycosylate OGA *in vitro*¹⁹. Inhibition of OGA using PUGNAc led to a robust increase in OGA glycosylation at Ser-405, raising the possibility that OGA activity may be regulated by OGT. Interestingly, OGT and OGA were recently shown to form a stable transcriptional regulatory complex, and Ser-405 is located within a region of OGA required for association with OGT²⁰.

Table 2 Identification and quantification of changes in *O*-GlcNAc glycosylation induced by PUGNAc

Protein	NCBI entry	Fold change ^a	Function	Peptide sequence ^b	Residues	MS method
BHC80	62645406	1.4	Neuronal gene repression, scaffolding	FTPTTLPTSQNSIHPVR	284–300	ETD
eIF4G	62658155	33	Translation elongation scaffolding	AQPPSSAASR	63–72	MS4
Nucleoporin 153	1709215	4.7	RNA binding and transport	KEELPQSSSAG	1004–1114	MS4
OGA	18777747	28.7	<i>N</i> -acetyl-D-glucosaminidase	QVAHSGAK	401–408	MS4
p66 β	67846054	40.3	Transcriptional repression	SISQSIGGQK	584–593	ETD
SRC-1	34863079	1.5	Coactivation of nuclear receptor transcription	INPSVNPGISPAHGVTR	188–204	ETD
Zinc finger RNA-binding protein	34854400	24.6	RNA-binding protein	AGYSQGATQYTQAQQAR	58–74	ETD
RecQ protein-like 4	17313266	N/D	DNA helicase	KQAAFGGSGPR	378–388	ETD

^a Fold change represents the observed heavy:light ratio averaged over all experiments. See Supplementary Methods for details on statistical analysis. ^b Potential glycosylation sites determined by ETD are shown in red. N/D, not detected

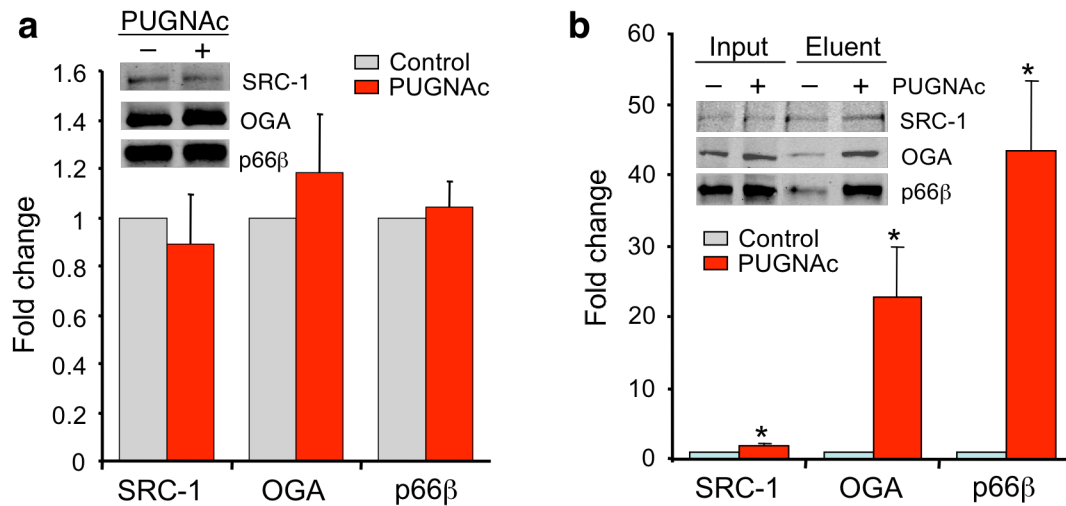


Figure 5: Quantification of *O*-GlcNAc glycosylation on intact proteins by immunoblotting and infrared imaging detection. **(a)** Minimal changes in the expression of SRC-1, OGA, and p66β were observed upon PUGNAc treatment of cortical neurons. Values represent quantification of 4-6 replicates, and a representative Western blot is shown for each protein. Data are mean \pm standard deviation (s.d). **(b)** *O*-GlcNAc glycosylation of SRC-1, OGA and p66β was stimulated upon PUGNAc treatment by 1.9 ± 0.3 -, 22.8 ± 7.0 -, and 43.3 ± 9.8 -fold, respectively. *O*-GlcNAc proteins from the lysates were chemoenzymatically labeled with the ketogalactose-biotin tag and selectively captured using streptavidin beads. Quantification was performed as described in the Methods, and values were corrected for any minor changes in protein expression levels shown in **Fig. 5a**. Data are mean \pm standard deviation (s.d). Statistical analysis was performed using the Student's *t*-test, $n = 3$, $*P < 0.05$. Input, lysates prior to streptavidin capture; Eluent, *O*-GlcNAc proteins captured by streptavidin

To rule out the possibility that the observed increases in *O*-GlcNAc glycosylation are due to altered protein expression, I immunoblotted cell lysates from neurons treated in the presence or absence of PUGNAc with all obtainable antibodies against the proteins of interest. Minimal changes in protein expression were detected upon PUGNAc treatment (**Fig. 5a**), suggesting that the observed changes are due to increased glycosylation. As further confirmation of our approach, I quantified the changes in *O*-GlcNAc levels using an alternative method. Specifically, I chemoenzymatically labeled *O*-GlcNAc proteins

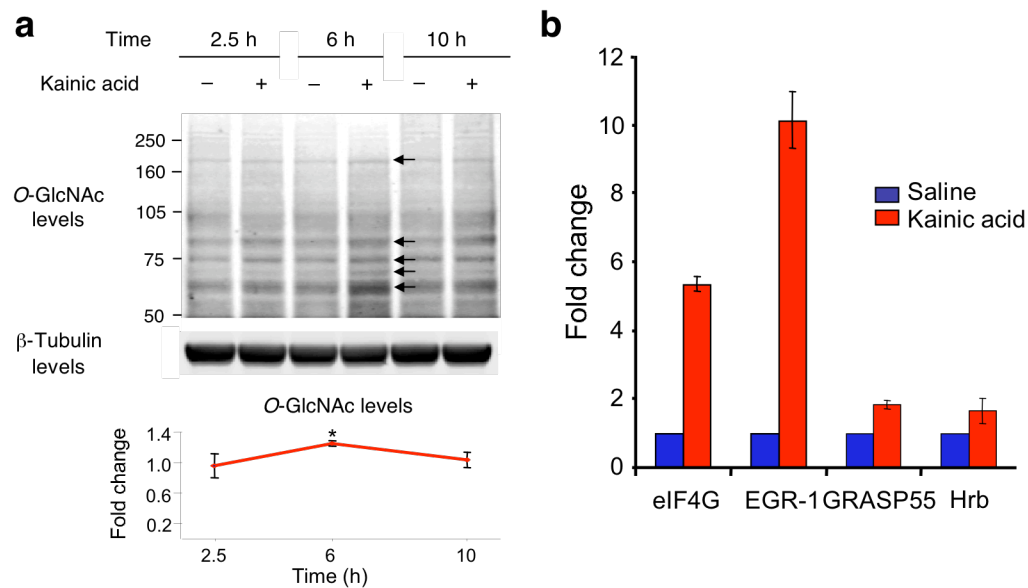


Figure 6: *O*-GlcNAc glycosylation is dynamically modulated by robust excitatory stimulation of the brain *in vivo* using kainic acid. **(a)** Overall *O*-GlcNAc glycosylation levels on several proteins in the cerebral cortex (indicated by arrows) are elevated at 6 h post-injection and then return to basal levels after 10 h, as measured using an anti-*O*-GlcNAc antibody. Data are mean \pm standard deviation (s.d). Statistical analysis was performed using the Student's *t*-test, $n = 3$, $*P < 0.05$. **(b)** Proteins identified using the QUIC-Tag method whose *O*-GlcNAc glycosylation levels increase by greater than 1.5-fold upon kainic acid stimulation. Cortical cell lysates were harvested at 6 h post-injection. Data are mean \pm s.d. Statistical analysis was performed using the Student's *t*-test, $n = 2 - 4$.

from cells treated with or without PUGNAc and captured the biotinylated proteins using streptavidin agarose. Following elution, I immunoblotted for specific proteins and quantified changes in *O*-GlcNAc based on the relative amounts of glycosylated protein captured by streptavidin. I found that PUGNAc treatment of neurons induced a 1.9 ± 0.3 -fold increase in *O*-GlcNAc glycosylation of SRC-1, consistent with the results obtained using our quantitative proteomics approach (**Fig. 5b**). Similarly, *O*-GlcNAc glycosylation was stimulated approximately 22.8 ± 7.0 -fold on OGA and 43.3 ± 9.8 -fold on p66 β . These results validate the quantitative proteomics methodology and highlight

the versatility of the chemoenzymatic platform for the detection of *O*-GlcNAc peptides or proteins by both MS and immunoblotting.

O*-GlcNAc Glycosylation Is Regulated by Excitatory Stimulation *In Vivo

Having demonstrated the reversibility of the *O*-GlcNAc modification in neurons, we next investigated whether *O*-GlcNAc glycosylation is induced *in vivo* by neuronal stimulation. Jessica Rexach and I intraperitoneally injected rats with kainic acid, a kainate-type glutamate receptor agonist that produces a robust excitatory stimulus of the brain. Kainic acid has been used to study excitatory pathways that induce gene expression and synaptic plasticity²¹ and to invoke seizures as a well-characterized model for temporal lobe epilepsy²². We dissected the cerebral cortices of kainic acid-treated rats at distinct behavioral time points: 2.5 h post-injection at peak of seizure, 6 h post-injection when animals had resumed some normal resting behavior, and 10 h post-injection when animals showed nearly identical behavior to saline-injected controls. Global changes in *O*-GlcNAc levels were measured by immunoblotting the cortical cell lysate with an anti-*O*-GlcNAc antibody. I found that *O*-GlcNAc levels on several proteins were elevated at 6 h post-injection and returned to basal levels by 10 h post-injection (**Fig. 6a**).

To identify proteins undergoing changes in *O*-GlcNAc glycosylation in response to kainic acid, Nelly applied our quantitative proteomics strategy to cortical lysates obtained 6 h post-injection. Thirteen of 83 *O*-GlcNAc peptides detected by MS underwent a robust, reproducible increase in response to kainic acid stimulation of rats. Specifically, the changes for these peptides were greater than 2σ over the mean of the 1:1

Table 3 Identification and quantification of changes in *O*-GlcNAc glycosylation induced by kainic acid

Protein	NCBI Entry	Fold Change ^a	s.d. ^b	n	Function	Peptide Sequence	Residues
EGR-1	6978799	10.1	± 0.9	2	gene transcription, stress response	ALVETSYPSQTTR	87-99
eIF4G	62658155	5.3	± 0.2	2	translation elongation	AQPPSSAASR	63-72
GRASP55	51259254	1.8	± 0.1	2	membrane protein transport, golgi stacking	VPTTVEDR	423-430
Hrb	90101424	1.6	± 0.4	4	RNA trafficking	SSSADFGSFSTSQSHQTASTVSK	291-313
bassoon	9506427	1.3	± 0.3	4	synaptic vesicle cycling	SPSTSSTHISYGQPPTTANYGSQ- TEELPHAPSGPAGSGR ^c	1402-1440
bassoon	9506427	1.5	± 0.1	2	synaptic vesicle cycling	ASGAGGPPPELPAGGAR	2283-2300
inositol polyphosphate-4-phosphatase	13591898	1.2	± 0.6	4	lipid phosphatase	SDQQPPVTR	177-186

^a Fold change represents the observed heavy/light ratio averaged over all experiments. See Supplementary Methods for details on statistical analysis.

^b Maximum absolute standard deviation (s.d.) calculated from g.s.d.

^c Peptide is also phosphorylated. See text for additional details.

standard peptides for multiple experiments. Using CAD tandem mass spectrometry, Scott successfully identified 4 of these proteins as eIF4G, the transcription factor early growth response-1 (EGR-1), the trafficking protein Golgi reassembly stacking protein 2 (GRASP55), and the HIV-1 Rev-binding protein (Hrb; **Fig. 6b** and **Table 3**). Interestingly, the same peptide of eIF4G that undergoes reversible glycosylation upon PUGNAc treatment also undergoes a change in glycosylation in response to kainic acid. Scott also sequenced 3 *O*-GlcNAc peptides that did not undergo reproducible changes in glycosylation (**Table 3**).

Kainic acid

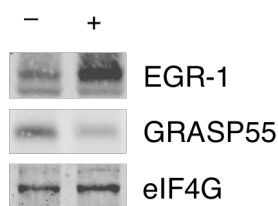


Figure 7: Expression levels of EGR-1, GRASP55, and eIF4G following kainic acid treatment of rats. Cortical neuronal lysates were obtained 6 h post-injection of kainic acid or PBS. EGR-1 expression changed by 1.8 ± 0.2 , GRASP55 expression by 0.61 ± 0.09 , and eIF4G expression by 1.5 ± 0.1 . Data represent the mean \pm s.d. for 3 experiments.

I confirmed that the observed increases in *O*-GlcNAc glycosylation were not due to enhanced protein expression by immunoblotting cortical lysates of kainic acid-treated or control PBS-treated rats with available antibodies against the proteins of interest. Consistent with previous reports that EGR-1 expression is upregulated approximately twofold in the cerebral cortex following kainic acid administration²³, I found that EGR-1 expression was elevated 1.8 ± 0.2 -fold at 6 h post-injection (**Fig. 7**). Given that *O*-GlcNAc glycosylation of EGR-1 is enhanced by 10.7-fold, protein expression changes

alone cannot account for the sizeable effect of kainic acid on EGR-1 glycosylation. Similarly, the change in eIF4G expression was modest (1.5 ± 0.1) relative to the change in its *O*-GlcNAc level (4.9 ± 0.7), and GRASP55 underwent a decrease in protein expression level with kainic acid treatment (0.61 ± 0.09). To our knowledge, these data represent the first demonstration that extracellular stimuli beyond glucose concentrations in the brain contribute to the dynamics of *O*-GlcNAc glycosylation.

Expanding the *O*-GlcNAc Proteome of the Brain

In addition to obtaining quantitative information on the dynamics of *O*-GlcNAc glycosylation, we also identified 20 *O*-GlcNAc peptides corresponding to 6 new and 12 previously characterized *O*-GlcNAc proteins from the brain (**Table 4**). Although changes

Table 4 *O*-GlcNAc glycosylated proteins identified from the cerebral cortex of kainic acid-stimulated rats

Protein	NCBI Entry	Function	Peptide Sequence	Residues
bassoon	9506427	synaptic vesicle cycling	VTQHFAK	1338-1444
CCR4-NOT4	34855140	global transcriptional regulation, mRNA metabolism	SNPVIPISSNHSAR	329-343
CRMP-2	599966	axonal guidance, neuronal polarity	TVTPASSAK ^a	512-520
erythrocyte protein band 4.1-like 1, isoform L	11067407	cytoskeletal protein	DVLTSTYGATAELTSTSTTHVTK	1460-1483
HCF	109511332	chromatin-associated factor	QPETYHYTTNTPTTAR	1232-1248
LMP-1	62988302	contains PDZ and LIM domain	AQPAQSKPKQK	28-37
MAP2b	547890	dynamic assembly of microtubules at dendrites	VADVPVSEATTVLGDVHSPAEGFVGENISGEEK	380-413
<i>O</i> -GlcNAcase	18777747	<i>N</i> -acetyl-D-glucosaminidase	QVAHSGAK	401-408
PDZ-GEF	34857578	GTP/GDP exchange factor for RAP1/2	SSIVSNSSFDSVPSVLHDER	1215-1233
phosphatidylinositol-binding clathrin assembly protein	16758324	regulation of clathrin assembly	SSGDVHLPISSDVSTFTTR	436-454
Rab3 GDP/GTP exchange protein	1947050	regulation of GTP/GDP exchange for Rab3 subfamily G proteins	SSSSTTASSSPSTIVHGAHSEPADSTEVGDK	699-729
Rad23b	60422770	translocation ubiquitinated proteins	AAAATTTATTTTSGGHPLEFLR	176-198
SH3p8	2293466	SH3 domain binding protein, synaptic vesicle cycling	ITASSSFR	283-290
SRC-1	34863079	coactivation of nuclear receptor transcription	INPSVNPGISPAHGVTTR	188-204
SynGAP	34098355	inhibitory regulation of Ras pathway, synaptic strength regulation	QHSQTPSTLNTPMPASER	1121-1138
Ythdf3	109466336	contains YTH domain	IGGDLTAAVTK	145-155

^a Peptide is also phosphorylated. See text for additional details.

in their glycosylation levels could not be accurately quantified due to low signal-to-noise ratios, these proteins further expand the *O*-GlcNAc proteome of the brain and highlight the abundance of the *O*-GlcNAc modification in neurons. For instance, we identified a glycosylated peptide on the collapsin response mediator protein-2 (CRMP-2), a protein critical for proper axonal development in neurons. We also observed the *O*-GlcNAc modification on several peptides of the large presynaptic scaffolding protein bassoon as well as the phosphatidylinositol-binding clathrin assembly protein. Finally, we found

several new *O*-GlcNAc-modified proteins such as the Rab3 guanine nucleotide exchange protein.

We have developed the first quantitative proteomics method to study the dynamics of *O*-GlcNAc glycosylation *in vivo*. Our QUIC-Tag approach combines the ability to selectively biotinylate and capture *O*-GlcNAc-modified proteins with a simple and efficient isotopic labeling strategy. When combined with tandem mass spectrometry, the method enables unambiguous identification and simultaneous quantification of individual *O*-GlcNAc glycosylation sites. Notably, the chemoenzymatic tagging method does not perturb endogenous *O*-GlcNAc glycosylation levels, unlike previously reported metabolic labeling approaches²⁴. The cells are rapidly lysed under denaturing conditions, and the physiological glycosylation state of proteins is preserved and captured by transfer of the ketogalactose-biotin tag. The isotopic labeling strategy has the advantage of being fast, high yielding and inexpensive relative to other methods. As it does not require metabolic labeling or multiple cell divisions for incorporation, the strategy can be readily applied to post-mitotic cells such as neurons or pancreatic islets, as well as to tissues harvested after *in vivo* stimulation. This enables *O*-GlcNAc glycosylation to be studied in more physiological settings and in key cell types where the modification is most highly abundant^{25, 26}.

Our approach has distinct advantages over existing methods for monitoring *O*-GlcNAc glycosylation levels. Although a few examples of site-specific *O*-GlcNAc antibodies have been reported^{27, 28}, such antibodies are limited in scope and are time-consuming and difficult to generate. As a result, many studies have utilized general *O*-

GlcNAc antibodies to detect global changes in *O*-GlcNAc glycosylation by immunoblotting^{11, 12}. These general *O*-GlcNAc antibodies are powerful for many applications, but they have limited sensitivity and do not enable direct identification of specific proteins or sites of modification. Recently, BEMAD (beta-elimination followed by Michael addition with dithiothreitol), a chemical derivatization technique used to identify *O*-GlcNAc and phosphorylation sites, has been coupled to isotopic labeling to study phosphorylation sites in complex mixtures following phosphatase treatment²⁹. However, the inherent promiscuity of β -elimination for any modified *O*-linked serine or threonine residues requires extensive internal controls to determine which *O*-linked species is being quantified. Overall, the scarcity of methods available for quantifying *O*-GlcNAc levels highlights the need for the development of new tools for identifying the proteins and pathways that regulate *O*-GlcNAc glycosylation.

In this study, we identified *O*-GlcNAc peptides of interest using two modes of peptide dissociation, CAD and ETD. By CAD, the chemoenzymatic tag produces a unique fragmentation pattern that permits definitive detection of *O*-GlcNAc-modified peptides. Peptides displaying the signature are then targeted for sequencing by MS⁴. In contrast to CAD, ETD generates product ions that retain the *O*-GlcNAc modification and thus can be used to identify exact sites of glycosylation within peptides. Moreover, because sequencing is conducted at the MS/MS stage, ETD forgoes the need for multiple additional stages of MS, which incur loss of signal at each stage. Unlike the related electron capture dissociation (ECD) strategy recently employed to map glycosylation sites that requires the use of FT instrumentation³⁰, ETD may be performed directly in appropriately modified ion trap mass spectrometers whose speed, sensitivity, and

accessibility to most laboratories make ETD an ideal emerging technology. Here, we report the first use of ETD technology to study *O*-GlcNAc glycosylation and demonstrate both sequencing and site identification of *O*-GlcNAc peptides from complex mixtures.

Our studies indicate that PUGNAc treatment of cortical neurons induces dramatic changes in *O*-GlcNAc glycosylation on specific proteins. These results suggest that *O*-GlcNAc glycosylation is highly reversible and may be rapidly cycled within neurons. Notably, we found that only a fraction of the *O*-GlcNAc-modified proteins undergo reversible glycosylation. Thus, OGT and OGA may be subject to complex cellular regulation analogous to that of kinases and phosphatases, such as the influence of interacting partners, subcellular targeting and post-translational modifications. The cycling of *O*-GlcNAc on certain substrates, coupled with more inactive, perhaps constitutive, forms of *O*-GlcNAc glycosylation, may allow for the finely-tuned, selective regulation of protein function in response to neuronal stimuli.

One of the proteins whose glycosylation level is significantly increased by PUGNAc treatment is the transcriptional repressor p66 β . p66 β interacts with histone tails and mediates transcriptional repression by the methyl-CpG-binding domain protein MBD2³¹. Our observation that p66 β is reversibly *O*-GlcNAc glycosylated reinforces growing evidence that *O*-GlcNAc plays an important role in the regulation of gene expression^{3, 4, 18, 25, 32, 33}. As p66 β appears to be sumoylated *in vivo* in a manner that affects its repression potential³⁴, our results also highlight a growing network of post-translational modifications that may be fundamental for the regulation of transcription, and it provides a new target with which to study this process.

We also identified changes in glycosylation on several proteins involved in the transport and translocation of mRNA. Such processes are of particular interest in neurons, where regulated transport of mRNA from the cell body to dendrites and dendritic translation of mRNA are involved in changes in synaptic strength that give rise to synaptic plasticity³⁵. In particular, we found reversible *O*-GlcNAc glycosylation on the zinc finger RNA-binding protein, which is associated with *staufen2* granules in neurons³⁶ and may be important in the early stages of RNA translocation from the nucleus to the dendrites. We also observed enhanced glycosylation of a peptide from the C-terminal domain of nucleoporin 153, a protein necessary for docking and trafficking of mRNA³⁷.

In addition to studying the reversibility of *O*-GlcNAc in neurons, we demonstrated for the first time that *O*-GlcNAc glycosylation is regulated *in vivo* by robust excitatory stimulation. For example, we found that EGR-1, an immediate early gene and transcription factor important for long-term memory formation³⁸ and cell survival³⁹, undergoes a tenfold increase in glycosylation upon kainic acid stimulation. As the site of glycosylation resides in the N-terminal transactivation domain of EGR-1, one possibility is that *O*-GlcNAc may influence the transactivation potential of EGR-1 and modulate the expression of genes such as the synapsins and proteasome components⁴⁰, which play critical roles in synaptic plasticity.

We also observed an increase in *O*-GlcNAc glycosylation on the translation factor eIF4G upon kainic acid stimulation. As kainic acid treatment induces excitotoxicity in addition to synaptic potentiation⁴¹ and suppressed translation is a known marker for neuronal excitotoxicity⁴², the potential regulation of eIF4G by *O*-GlcNAc glycosylation

may represent a stress-induced response. It will be important to examine whether other cellular stresses induce glycosylation of eIF4G and other proteins to modulate translation and neuronal survival. Consistent with this possibility, other components of the translational machinery have been shown to be *O*-GlcNAc modified, such as p67, which binds to the eukaryotic initiation factor 2 α (eIF2 α) in its glycosylated form and promotes protein synthesis by preventing inhibitory phosphorylation of eIF2 α ⁴³.

The ability of *O*-GlcNAc to respond to specific extracellular stimuli suggests a potential role for the modification in mediating neuronal communication. This notion is supported by the identification of a growing number of *O*-GlcNAc glycosylated proteins involved in neuronal signaling and synaptic plasticity^{3,30}. In the present study, we further expand the *O*-GlcNAc proteome of the brain to include proteins involved in synaptic vesicle trafficking, including Rab3 GEP, a protein involved in neurotransmitter release, and phosphatidylinositol clathrin protein, which mediates synaptic vesicle endocytosis. In keeping with recent work by Vosseller and colleagues³⁰, we find that the presynaptic protein bassoon, which is necessary for the creation of stable synapses and proper neuronal communication, is *O*-GlcNAc modified. We also identify *O*-GlcNAc glycosylation on signal transduction proteins such as the kinase AAK1, which is involved in clathrin-mediated synaptic vesicle endocytosis, and the synaptic Ras GTPase activating protein SynGAP, which plays a critical role in AMPA (alpha-amino-3-hydroxy-5-methyl-4-isoxazolepropionic acid) receptor trafficking and synapse formation.

Finally, our work highlights the emergent interplay between *O*-GlcNAc glycosylation and phosphorylation. For example, we identified a glycosylated peptide on bassoon that is likewise phosphorylated *in vivo*⁴⁴. Moreover, the axonal guidance protein

CRMP-2 is phosphorylated at two residues within the glycopeptide identified in our studies⁴⁵. Interestingly, when hyperphosphorylated within the residues of this peptide, CRMP-2 appears as a component of the neurofibrillary tangles associated with Alzheimer's disease (AD). This is reminiscent of the microtubule-associated protein tau, which is also *O*-GlcNAc glycosylated but exists in hyperphosphorylated form in the AD brain⁴⁶. Deciphering the mechanisms that regulate the interplay of glycosylation and phosphorylation for these and other proteins may have important ramifications for the study of neuronal signaling and neurodegenerative disorders.

In summary, we demonstrate a new quantitative proteomics strategy for studying the dynamics of *O*-GlcNAc glycosylation. Our findings reveal that the *O*-GlcNAc modification is reversible and dynamically regulated in neurons, and is found on many proteins essential for synaptic function. These observations, along with the discovery that excitatory stimulation can induce *O*-GlcNAc glycosylation in the brain, suggest that *O*-GlcNAc may represent an important post-translational modification for the regulation of neuronal communication. We envision that further application of this methodology will significantly advance our understanding of the regulation of *O*-GlcNAc glycosylation in the nervous system.

Methods

PUGNAc treatment of cortical cultures. Cortical neuronal cultures were prepared from embryonic day 18 or 19 Sprague Dawley rats as described⁴⁷. Cells ($8-12 \times 10^6$) were plated on 100-mm culture dishes coated with a 0.1 mg ml^{-1} sterile-filtered, aqueous

solution of poly-DL-lysine (Sigma). Cells were maintained for 4 days at 5% CO₂/37 °C. The media was replaced on the second day and immediately prior to PUGNAc treatment. PUGNAc (Toronto Research Chemicals) was added to the cells at a final concentration of 100 μM (10 mM aqueous stock, sterile-filtered). After 12 h of incubation, the cells were scraped off the plates and pelleted. The media was removed by aspiration, and the cell pellet was washed with 1 ml of HEPES-buffered saline and lysed as described below. Basal neurons were treated identically, except that a water control was used instead of PUGNAc.

Kainic acid administration. Male Long Evans rats (7 weeks-old, 190–200 g) were injected intraperitoneally with either 10–11 mg kg⁻¹ of kainic acid (5 mg ml⁻¹ in phosphate buffered saline (PBS); Axxora) or PBS as a control. Animals were housed separately and closely monitored for behavioral changes characteristic of seizure activity. Animals were sacrificed at 3 time points, with paired animals demonstrating similar kainic-acid induced behavior: 2.5 h post-injection, when animals were displaying class 4 seizure behavior, 6 h post-injection, when seizure activity was subsiding and animals were displaying some similarity to controls, and 10 h post-injection, when animals were largely indistinguishable from controls. At each time point, the cortices were dissected, flash frozen in liquid N₂ and stored at -80 °C until further use. All animal protocols were approved by the Institutional Animal Care and Use Committee at Caltech, and the procedures were performed in accordance with the Public Health Service Policy on Humane Care and Use of Laboratory Animals.

Dimethyl labeling. Protein extracts from PUGNAc-treated cortical neurons and kainic-acid treated brain samples were prepared, chemoenzymatically labeled, and proteolytically digested as described below. Digested extracts were desalted using a Sep-Pak C18 cartridge (1 cc bed volume; Waters). Peptides were eluted in 500 μ l of 60% aqueous CH_3CN , concentrated by speedvac to a volume of 50 μ l, and diluted with 450 μ l of 1 M HEPES pH 7.5. To begin the reactions, the samples were mixed with 40 μ l of a 600 mM stock of NaCNBH_3 or NaCNBD_3 (Sigma) in water, followed by 40 μ l of 4% aqueous formaldehyde (Mallinckrodt Chemicals) or 40 μ l of 4% aqueous formaldehyde-d₂ (Sigma). The reactions were briefly vortexed, allowed to proceed for 10 min at room temperature, and then quenched by acidification with 100% AcOH to a pH <4.5. Dimethylated peptides were desalted using a Sep-Pak C18 cartridge (1 cc bed volume), and the eluents (500 μ l in 60% aqueous CH_3CN , 0.1% AcOH) were concentrated by speedvac to a volume of 100 μ l.

Cation exchange and avidin chromatography. Cation exchange chromatography (Applied Biosystems) was performed on dimethylated peptides as described by the manufacturer, except that peptides were eluted with a step gradient of 100 mM, 250 mM, and 350 mM KCl in 5 mM KH_2PO_4 containing 25% CH_3CN . Fractionated peptides were enriched via monomeric avidin chromatography (Applied Biosystems) as follows: peptides were loaded onto the avidin column as described by the manufacturer and washed with 2 ml of 2X PBS (1X PBS final concentration: 10.1 mM Na_2HPO_4 , 1.76 mM KH_2PO_4 , 137 mM NaCl, 2.7 mM KCl, pH 6.7), 2 ml of 1X PBS, 1.5 ml of manufacturer

wash buffer 2 and 1 ml of ddH₂O. Avidin-enriched peptides were eluted as described by the manufacturer.

Orbitrap MS analysis and ETD analysis. Automated nanoscale reversed-phase HPLC/ESI/MS was performed as described below and previously³. For data-dependent experiments, the mass spectrometer was programmed to record a full-scan ESI mass spectrum (m/z 650–2000, ions detected in orbitrap mass spectrometer with a resolution set to 100000) followed by five data-dependent MS/MS scans (relative collision energy = 35%; 3.5 Da isolation window). Precursor ion masses for candidate glycosylated peptides were identified by a computer algorithm (Charge Loss Scanner; developed in-house with Visual Basic 6.0) that inspected product ion spectra for peaks corresponding to losses of the ketogalactose-biotin and GlcNAc-ketogalactose-biotin moieties. Up to eight candidate peptides at a time were analyzed in subsequent targeted MS⁴ experiments to derive sequence information.

For all MS experiments, the electrospray voltage was set at 1.8 kV and the heated capillary was maintained at 250 °C. For database analysis to identify *O*-GlcNAc proteins, Bioworks Browser 3.2SR1 (ThermoElectron) software was used to create files from MS⁴ data and ETD MS/MS data. These files were then directly queried, using the SEQUEST algorithm (ThermoElectron), against amino acid sequences in the NCBI rat/mouse protein database.

Quantification was conducted by generating single ion chromatograms from the orbitrap MS scans for candidate *O*-GlcNAc peptides. Peak areas of isotopic clusters were derived using Xcalibur 1.4 software (ThermoElectron) and relative ratios were

normalized against the mean relative ratio of standard peptides. Statistical analysis is described in detail below.

MS/MS experiments by ETD were conducted on a modified LTQ mass spectrometer. A chemical ionization source was added to the rear side of the LTQ to allow for the introduction of fluoranthene radical anions for ETD reactions. For data-dependent experiments, the mass spectrometer was programmed to record a full-scan ESI mass spectrum (m/z 650–2000) followed by five data-dependent MS/MS scans (70–100 ms ETD activation; 3.5 Da isolation window). In some cases, targeted MS/MS was conducted on up to eight candidate peptides that had demonstrated the signature ketogalactose-biotin loss during CAD MS/MS. All sequenced peptides were manually verified.

Chemoenzymatic labeling and streptavidin capture of *O*-GlcNAc proteins.

Chemoenzymatic labeling was performed on neuronal lysates as described above. After reaction with the aminoxy biotin derivative, proteins were dialyzed (1 x 10 h, 2 x 3 h) into 7 M urea, 10 mM HEPES, pH 7.5 at room temperature followed by 10 mM HEPES pH 7.5, 100 mM NaCl, 0.2% Triton-X 100 (2 x 2 h, 1 x 10 h) at 4 °C. Fresh PMSF (1 mM) was added at each stage of dialysis. Proteins were captured on streptavidin beads as previously described⁴ and probed by immunoblotting.

Western blotting. Lysates were resolved by SDS-PAGE, transferred to nitrocellulose membranes and immunoblotted as described previously⁴. Total *O*-GlcNAc levels were monitored using the anti-*O*-GlcNAc antibody CTD110.6 (Covance, 1:5000). The

following primary antibodies were also used: EGR-1 (Upstate Biotechnology, 1:1000), GRASP-55 (BD Transduction Laboratories, 1:1000), eIF4G (Santa Cruz, 1:100), OGA (a kind gift from Prof. Sidney Whiteheart, University of Kentucky, 1:1000), p66 β (Upstate, 1:500), and SRC-1 (Santa Cruz, 1:100). After incubation with the secondary antibodies IRDye 800 goat anti-rabbit (Rockland Immunochemicals) or Alexa Fluor 680 goat anti-mouse (Molecular Probes), proteins were visualized and quantified using the Odyssey infrared imaging system (LI-COR Biosciences). To quantify differences in *O*-GlcNAc levels, we measured the relative intensities of the input bands (lysate prior to streptavidin capture) and eluent bands (lysate after streptavidin capture) using Odyssey imaging software (Version 2.1). For each sample, we normalized the eluent signals to the input signals, and the resulting values from control reactions lacking GalT were subtracted from those values obtained from reactions containing GalT to correct for any nonspecific background.

Statistical analysis. Quantification was conducted by generating single ion chromatograms from the orbitrap MS scans for candidate *O*-GlcNAc peptides. Peak areas of isotopic clusters were derived using Xcalibur 1.4 software. Mean values, standard deviations and confidence intervals were calculated using the program Excel on log-transformed ratios and reported in the original scale as previously described^{2,3}. We used the geometric standard deviation (g.s.d.) to calculate maximum absolute standard deviations. Standard peptide ratios were tested for goodness of fit to the log-normal distribution via the D'Agostino-Pearson omnibus test and were used to determine the confidence with which changes in experimental peptides could be detected.

Experimental peptide ratios were normalized against the slope of the linear regression produced by the heavy vs. light forms of standard peptides within experiments.

References

1. Khidekel, N. *et al.* A chemoenzymatic approach toward the rapid and sensitive detection of *O*-GlcNAc posttranslational modifications. *J. Am. Chem. Soc.* **125**, 16162-16163 (2003).
2. Hsu, J.L., Huang, S.Y., Chow, N.H. & Chen, S.H. Stable-isotope dimethyl labeling for quantitative proteomics. *Anal. Chem.* **75**, 6843-6852 (2003).
3. Khidekel, N., Ficarro, S.B., Peters, E.C. & Hsieh-Wilson, L.C. Exploring the *O*-GlcNAc proteome: direct identification of *O*-GlcNAc-modified proteins from the brain. *Proc. Natl. Acad. Sci. USA* **101**, 13132-13137 (2004).
4. Tai, H.C., Khidekel, N., Ficarro, S.B., Peters, E.C. & Hsieh-Wilson, L.C. Parallel identification of *O*-GlcNAc-modified proteins from cell lysates. *J. Am. Chem. Soc.* **126**, 10500-10501 (2004).
5. Chalkley, R.J. & Burlingame, A.L. Identification of GlcNAcylation sites of peptides and alpha-crystallin using Q-TOF mass spectrometry. *J. Am. Soc. Mass Spectrom.* **12**, 1106-1113 (2001).
6. Makarov, A., Denisov, E., Lange, O. & Horning, S. Dynamic Range of Mass Accuracy in LTQ Orbitrap Hybrid Mass Spectrometer. *J. Am. Soc. Mass Spectrom.* **17**, 977-982 (2006).
7. Roquemore, E.P., Chevrier, M.R., Cotter, R.J. & Hart, G.W. Dynamic *O*-GlcNAcylation of the small heat shock protein alpha B-crystallin. *Biochemistry* **35**, 3578-3586 (1996).
8. Zhang, R., Sioma, C.S., Wang, S. & Regnier, F.E. Fractionation of isotopically labeled peptides in quantitative proteomics. *Anal. Chem.* **73**, 5142-5149 (2001).
9. Ong, S.E., Mittler, G. & Mann, M. Identifying and quantifying in vivo methylation sites by heavy methyl SILAC. *Nat. Methods* **1**, 119-126 (2004).
10. Ross, P.L. *et al.* Multiplexed protein quantitation in *Saccharomyces cerevisiae* using amine-reactive isobaric tagging reagents. *Mol. Cell. Proteomics* **3**, 1154-1169 (2004).
11. Kneass, Z.T. & Marchase, R.B. Neutrophils exhibit rapid agonist-induced increases in protein-associated *O*-GlcNAc. *J. Biol. Chem.* **279**, 45759-45765 (2004).
12. Zachara, N.E. *et al.* Dynamic *O*-GlcNAc modification of nucleocytoplasmic proteins in response to stress. A survival response of mammalian cells. *J. Biol. Chem.* **279**, 30133-30142 (2004).
13. Haltiwanger, R.S., Grove, K. & Philipsberg, G.A. Modulation of *O*-linked *N*-acetylglucosamine levels on nuclear and cytoplasmic proteins in vivo using the peptide *O*-GlcNAc-beta-*N*-acetylglucosaminidase inhibitor *O*-(2-acetamido-2-deoxy-D-glucopyranosylidene)amino-*N*-phenylcarbamate. *J. Biol. Chem.* **273**, 3611-3617 (1998).
14. Syka, J.E., Coon, J.J., Schroeder, M.J., Shabanowitz, J. & Hunt, D.F. Peptide and protein sequence analysis by electron transfer dissociation mass spectrometry. *Proc. Natl. Acad. Sci. USA* **101**, 9528-9533 (2004).
15. Coon, J.J., Syka, J.E.P., Schwartz, J.C., Shabanowitz, J. & Hunt, D.F. Anion dependence in the partitioning between proton and electron transfer in ion/ion reactions. *Int. J. Mass Spectrom.* **236**, 33-42 (2004).

16. Hogan, J.M., Pitteri, S.J., Chrisman, P.A. & McLuckey, S.A. Complementary structural information from a tryptic *N*-linked glycopeptide via electron transfer ion/ion reactions and collision-induced dissociation. *J. Proteome Res.* **4**, 628-632 (2005).
17. Swaney, D.L. *et al.* Supplemental activation method for high-efficiency electron-transfer dissociation of doubly protonated peptide precursors. *Anal Chem* **79**, 477-485 (2007).
18. Love, D.C. & Hanover, J.A. The hexosamine signaling pathway: deciphering the "*O*-GlcNAc code". *Sci. STKE* **2005**, re13 (2005).
19. Lazarus, B.D., Love, D.C. & Hanover, J.A. Recombinant *O*-GlcNAc transferase isoforms: identification of *O*-GlcNAcase, yes tyrosine kinase, and tau as isoform-specific substrates. *Glycobiology* **16**, 415-421 (2006).
20. Whisenhunt, T.R. *et al.* Disrupting the enzyme complex regulating *O*-GlcNAcylation blocks signaling and development. *Glycobiology* **16**, 551-563 (2006).
21. Nedivi, E., Hevroni, D., Naot, D., Israeli, D. & Citri, Y. Numerous candidate plasticity-related genes revealed by differential cDNA cloning. *Nature* **363**, 718-722 (1993).
22. Ben-Ari, Y. & Cossart, R. Kainate, a double agent that generates seizures: two decades of progress. *Trends Neurosci.* **23**, 580-587 (2000).
23. Beckmann, A.M., Davidson, M.S., Goodenough, S. & Wilce, P.A. Differential expression of Egr-1-like DNA-binding activities in the naive rat brain and after excitatory stimulation. *J. Neurochem.* **69**, 2227-2237 (1997).
24. Nandi, A. *et al.* Global identification of *O*-GlcNAc-modified proteins. *Anal. Chem.* **78**, 452-458 (2006).
25. Iyer, S.P. & Hart, G.W. Dynamic nuclear and cytoplasmic glycosylation: enzymes of *O*-GlcNAc cycling. *Biochemistry* **42**, 2493-2499 (2003).
26. Cole, R.N. & Hart, G.W. Cytosolic *O*-glycosylation is abundant in nerve terminals. *J. Neurochem.* **79**, 1080-1089 (2001).
27. Kamemura, K., Hayes, B.K., Comer, F.I. & Hart, G.W. Dynamic interplay between *O*-glycosylation and *O*-phosphorylation of nucleocytoplasmic proteins: alternative glycosylation/phosphorylation of THR-58, a known mutational hot spot of c-Myc in lymphomas, is regulated by mitogens. *J. Biol. Chem.* **277**, 19229-19235 (2002).
28. Ludemann, N. *et al.* *O*-glycosylation of the tail domain of neurofilament protein M in human neurons and in spinal cord tissue of a rat model of amyotrophic lateral sclerosis (ALS). *J. Biol. Chem.* **280**, 31648-31658 (2005).
29. Vosseller, K. *et al.* Quantitative analysis of both protein expression and serine / threonine post-translational modifications through stable isotope labeling with dithiothreitol. *Proteomics* **5**, 388-398 (2005).
30. Vosseller, K. *et al.* *O*-linked *N*-acetylglucosamine proteomics of postsynaptic density preparations using lectin weak affinity chromatography and mass spectrometry. *Mol. Cell. Proteomics* **5**, 923-934 (2006).
31. Brackertz, M., Gong, Z., Leers, J. & Renkawitz, R. p66alpha and p66beta of the Mi-2/NuRD complex mediate MBD2 and histone interaction. *Nucleic Acids Res.* **34**, 397-406 (2006).
32. Lamarre-Vincent, N. & Hsieh-Wilson, L.C. Dynamic glycosylation of the transcription factor CREB: a potential role in gene regulation. *J. Am. Chem. Soc.* **125**, 6612-6613 (2003).
33. Yang, X. *et al.* *O*-linkage of *N*-acetylglucosamine to Sp1 activation domain inhibits its transcriptional capability. *Proc. Natl. Acad. Sci. USA* **98**, 6611-6616 (2001).

34. Gong, Z., Brackertz, M. & Renkawitz, R. SUMO modification enhances p66-mediated transcriptional repression of the Mi-2/NuRD complex. *Mol. Cell. Biol.* **26**, 4519-4528 (2006).
35. Ule, J. & Darnell, R.B. RNA binding proteins and the regulation of neuronal synaptic plasticity. *Curr. Opin. Neurobiol.* **16**, 102-110 (2006).
36. Elvira, G., Massie, B. & DesGroseillers, L. The zinc-finger protein ZFR is critical for Staufien 2 isoform specific nucleocytoplasmic shuttling in neurons. *J. Neurochem.* **96**, 105-117 (2006).
37. Bastos, R., Lin, A., Enarson, M. & Burke, B. Targeting and function in mRNA export of nuclear pore complex protein Nup153. *J. Cell Biol.* **134**, 1141-1156 (1996).
38. Jones, M.W. *et al.* A requirement for the immediate early gene Zif268 in the expression of late LTP and long-term memories. *Nat. Neurosci.* **4**, 289-296 (2001).
39. Thiel, G. & Cibelli, G. Regulation of life and death by the zinc finger transcription factor Egr-1. *J. Cell. Physiol.* **193**, 287-292 (2002).
40. James, A.B., Conway, A.M. & Morris, B.J. Genomic profiling of the neuronal target genes of the plasticity-related transcription factor -- Zif268. *J. Neurochem.* **95**, 796-810 (2005).
41. Wang, Q., Yu, S., Simonyi, A., Sun, G.Y. & Sun, A.Y. Kainic acid-mediated excitotoxicity as a model for neurodegeneration. *Mol. Neurobiol.* **31**, 3-16 (2005).
42. Marin, P. *et al.* Glutamate-dependent phosphorylation of elongation factor-2 and inhibition of protein synthesis in neurons. *J. Neurosci.* **17**, 3445-3454 (1997).
43. Datta, R., Choudhury, P., Ghosh, A. & Datta, B. A glycosylation site, 60SGTS63, of p67 is required for its ability to regulate the phosphorylation and activity of eukaryotic initiation factor 2alpha. *Biochemistry* **42**, 5453-5460 (2003).
44. Collins, M.O. *et al.* Proteomic analysis of in vivo phosphorylated synaptic proteins. *J. Biol. Chem.* **280**, 5972-5982 (2005).
45. Gu, Y., Hamajima, N. & Ihara, Y. Neurofibrillary tangle-associated collapsin response mediator protein-2 (CRMP-2) is highly phosphorylated on Thr-509, Ser-518, and Ser-522. *Biochemistry* **39**, 4267-4275 (2000).
46. Liu, F., Iqbal, K., Grundke-Iqbal, I., Hart, G.W. & Gong, C.X. O-GlcNAcylation regulates phosphorylation of tau: a mechanism involved in Alzheimer's disease. *Proc. Natl. Acad. Sci. USA* **101**, 10804-10809 (2004).
47. Gama, C.I. *et al.* Sulfation patterns of glycosaminoglycans encode molecular recognition and activity. *Nat. Chem. Biol.* **2**, 467-473 (2006).